Horizon 2020 Programme

METIS

Research and Innovation Action (RIA)

This project has received funding from the European Union's Horizon 2020 research and innovation programme under grant agreement No 945121

Start date : 2020-09-01 Duration : 48 Months

Methodology for selecting ensembles of rock-hazard consistent ground motions suitable for fragility curves computations for clustered seismicity and dataset

Authors : Mrs. Paolo BAZZURRO (IUSS), Sipcic Nevena; García de Quevedo Inarritu Pablo, Kohrangi Mohsen, Bazzurro Paolo

METIS - Contract Number: 945121

Project officer: Katerina PTACKOVA

Document title	Methodology for selecting ensembles of rock-hazard consistent ground motions suitable for fragility curves computations for clustered seismicity and dataset
Author(s)	Mrs. Paolo BAZZURRO, Sipcic Nevena; García de Quevedo Inarritu Pablo, Kohrangi Mohsen, Bazzurro Paolo
Number of pages	22
Document type	Deliverable
Work Package	WP5
Document number	D5.2
Issued by	IUSS
Date of completion	2023-05-26 16:41:40
Dissemination level	Public

Summary

The work presented in this Report is part of WP5, which focuses on a selection of earthquake ground motion record sets both consistent with the hazard at the site of interest, as estimated by WP4, and also adequate for structural response analysis, performed by WP6. The previous Deliverable D5.1 addressed the hazard consistency for the mainshock-only case and investigated some long-standing issues vexing the selection of ground motion records for fragility analysis, such as mixing soil and rock motions, mixing synthetic and real motions, and using scaled motions to different extents. In this Report, we focus on the record selection in the context of clustered seismicity. We outline the state-of-the-art record selection methods for clustered seismicity and describe the framework proposed by (Papadopoulos et al., 2020). This framework ensures that the selected aftershock records have characteristics consistent (in terms of causal parameters and spectral shape) with the selected mainshock records. The suites of mainshock-aftershock records selected via the proposed methodology will then be used in WP6 to estimate the structural response and derive fragility curves for systems, structures and components (SSCs) of nuclear power plants (NPPs) that are dependent on the damage observed after the mainshock event.

Approval

Date	By
2023-05-26 16:42:42	Mrs. Paolo BAZZURRO (IUSS)
2023-05-26 17:33:55	Dr. Irmela ZENTNER (EDF)

METIS

Seismic Risk Assessment
for Nuclear Safety

Research & Innovation Action

NFRP-2019-2020

Methodology for selecting ensembles of rock-hazard-consistent ground motions suitable for fragility curve computations for clustered seismicity and datasets for WP6

Deliverable D5.2

Version N°2

Authors:

Šipčić Nevena

García de Quevedo Iñarritu Pablo

Kohrangi Mohsen

Bazzurro Paolo

Disclaimer

Document Information

Grant agreement	945121
Project title	Methods And Tools Innovations For Seismic Risk Assessment
Project acronym	METIS
Project coordinator	Dr. Irmela Zentner, EDF
Project duration	1st September 2020 – 31st August 2024 (48 months)
Related work package	WP5 - Ground motion selection for engineering analyses, including site response
Related task(s)	Task 5.2 - Methodology for site-specific rock-hazard-consistent record selection for clustered seismicity
Lead organisation	IUSS
Contributing partner(s)	IRSN, GEM, NTUA
Due date	31st August 2022
Submission date	26th May 2023
Dissemination level	

History

Version	Submitted by	Reviewed by	Date	Comments
N°1	Paolo Bazzurro	Matjaž Dolšek	09/05/2023	
N°2	Paolo Bazzurro			

Table of Contents

List of figures

List of tables

Abbreviations and Acronyms

Acronym	Description
PSHA	Probabilistic seismic hazard analysis
AS	Aftershock
CMS	Conditional mean spectrum
CS	Conditional spectrum
DB	Database
ETAS	Epidemic-Type Aftershock Sequence
GCIM	Generalized conditional intensity measure
GM	Ground motion
GMPM	Ground motion prediction model
GR	Gutenberg – Richter
IM	Intensity measure
IML	Intensity level
MAF	Mean annual frequency
MLE	Maximum likelihood estimation
MS	Mainshock
MSAS-CS	Mainshock-consistent aftershock conditional spectrum
NRTHA	Nonlinear response time history analysis
NPP	Nuclear power plant
PBEE	Performance-based earthquake engineering
PGA	Peak ground acceleration
poe	Probability of exceedance
PSHA	Probabilistic seismic hazard analysis
Rjb	Joyner and Boore distance
Rrup	Rupture distance
Sa	Spectral acceleration
SSC	Systems, structures and components
UHS	Uniform hazard spectrum
V_{s30}	Average shear wave velocity in the upper 30m
WP	Work package

Summary

The work presented in this Report is part of WP5, which focuses on a selection of earthquake ground motion record sets both consistent with the hazard at the site of interest, as estimated by WP4, and also adequate for structural response analysis, performed by WP6. The previous Deliverable D5.1 addressed the hazard consistency for the mainshock-only case and investigated some long-standing issues vexing the selection of ground motion records for fragility analysis, such as mixing soil and rock motions, mixing synthetic and real motions, and using scaled motions to different extents. In this Report, we focus on the record selection in the context of clustered seismicity.

We outline the state-of-the-art record selection methods for clustered seismicity and describe the framework proposed by (Papadopoulos et al., 2020). This framework ensures that the selected aftershock records have characteristics consistent (in terms of causal parameters and spectral shape) with the selected mainshock records. The suites of mainshock-aftershock records selected via the proposed methodology will then be used in WP6 to estimate the structural response and derive fragility curves for systems, structures and components (SSCs) of nuclear power plants (NPPs) that are dependent on the damage observed after the mainshock event.

Keywords

Ground motion record selection, hazard consistency, clustered seismicity, correlation coefficients

Introduction

Performance-Based Earthquake Engineering (PBEE) (Cornell & Krawinkler, 2000) focuses on the probabilistic assessment of the performance of structures subjected to earthquakes and separates the contributions from seismic hazard analysis and structural analysis. Within that framework, the seismic hazard at a site is defined by the Mean Annual Frequency (*MAF*) of exceeding certain levels of a conditioning ground motion (GM) Intensity Measure (*IM*) from all seismic scenarios that contribute to the hazard. This procedure is usually referred to as Probabilistic Seismic Hazard Analysis, or PSHA (e.g., McGuire, 2004). The structural response assessment is traditionally carried out via sets of fragility functions, which are conditioned on a specific *IM*, for different limit states. In the absence of empirical data to derive fragility curves from either the field or shake table tests, it is common to perform nonlinear response history analysis (*NLRHA*) using selected sets of ground motions. For these fragility curves to be robust and fit for purpose, such record sets should be statistically consistent with the motions that the structure may experience at the site in its intended lifetime. Loosely speaking, this concept is referred to as "hazard consistency" (Lin et al., 2013). If that does not happen, the ensuing fragility curves may be affected by an unknown bias large enough to render them unsuitable for practical application (Kohrangi et al., 2017). Hence, to ensure hazard consistency, sets of records should be carefully selected to avoid inaccurate or biased fragility curves, and in turn, risk estimates.

The objective of WP5 in the METIS project is to ensure that hazard consistency is attained by selecting appropriate ground motions representative of the hazard at the site on rock conditions following the outputs of WP4. The set of selected ground motions is then used as input for site response analysis to obtain ground motions at the soil surface for the specific site under consideration (Task 5.3). This results in unbiased and robust estimates of fragility curves (WP6) tailored for the given site.

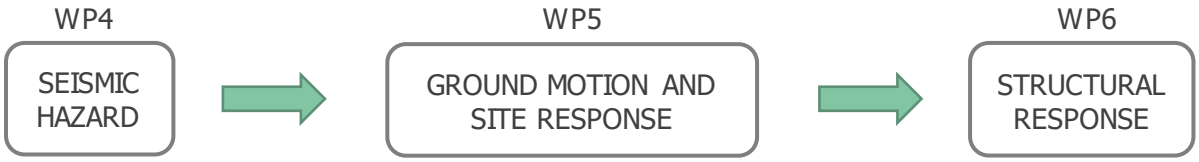

Figure 1: WP5 in the METIS workflow

In the past, several seismic sequences (e.g., Christchurch 2011, Central Italy 2016-2017, Turkey 2023 to mention only the most recent) showed that the earthquake sequences pose an additional risk to society as the financial losses increase when compared to cases characterized by only one main event (i.e., mainshock only cases). Traditional approaches for seismic risk assessment focus solely on mainshocks, a practice that can lead to a significant underestimation of seismic risk. This is the case especially in the aftermath of major events that invariably are followed by a cluster of aftershocks, several of which could be damaging. This issue has been long recognized and several researchers have been studying how to incorporate clustered seismicity into risk assessment both in terms of hazard and vulnerability. The increase in seismic hazard due to the consideration of seismic sequences is studied in the WP4 (Task 4.4.2) and, therefore, it will not be discussed here. The potential underestimation of structural vulnerability comes as a consequence of the damage accumulation during the sequences. To quantify this effect, the concept of fragility functions conditioned on the damage experienced after the mainshock (MS) has been introduced[1]. To derive damage-dependent fragility curves analytically, NLRHAs have to be performed by subjecting the structure to both the MS and aftershock (AS) ground motions in a back-to-back fashion.

Due to the scarcity of MS-AS ground motions (particularly in the high-intensity range) recorded at the same station, several authors decided to use MS ground motions to represent the shaking caused by

[1] In a cluster of earthquakes, the first damaging earthquake may not be the largest magnitude event (namely the mainshock) of the sequence. For example, in the Central Italy sequence of 2016-17 the first damaging event, the M6 on 08/24/2016 that leveled the town of Amatrice, was a foreshock of the M6.5 earthquake that occurred on 10/30/2016, which can be considered as the mainshock of the sequence.

both the MS and the AS events (e.g., Amadio et al., 2003; Raghunandan et al., 2015; Wen et al., 2017). To make these scenarios more realistic, various studies have attempted to enhance the accuracy of the simulations by either randomly pairing mainshock ground motions or scaling down the aftershock ground motion (Aljawhari et al., 2020; Jeon et al., 2015; Ryu et al., 2011). Some of the first efforts to construct MS-AS sequences consistent with the aftershock recurrence were made by (Sunasaka & Kiremidjian, 1993), and later extended by (Li & Ellingwood, 2007). (Goda & Taylor, 2012) developed a methodology that uses the generalized Omori model (Reasenberg & Jones, 1989) to model aftershock recurrence, sampling AS magnitudes and inter-arrival times to select a compatible record. The importance of using real ground motions has been studied by (Ruiz-García & Negrete-Manriquez, 2011), who concluded that using artificial seismic sequences could lead to overestimations in maximum lateral drift demand and record-to-record variability. (Li et al., 2014) considered and compared three approaches: (1) the use of as-recorded mainshock-aftershock sequences; (2) the use of repeated seismic sequences, where the same mainshock ground motion is used as aftershock; (3) the use of randomized seismic sequences which are generated while taking into account the differences in ground motion features of the mainshock and aftershock. The study showed that the variation in collapse capacity may be underestimated unless real MS-AS sequences are used.

While the importance of site dependency in selecting ground motions for response analysis has been recognized and studied by several researchers (Bradley, 2010; Kohrangi et al., 2017; Lin et al., 2013), as discussed in Deliverable 5.1 (D5.1), there is comparatively less research on this topic concerning seismic sequences. Given the correlation between the MS and AS causal parameters, as well as the "similarity" in the spectral shape of MS and AS ground motions at the same station, it is reasonable to assume that site dependency is also relevant for clustered seismicity. Nevertheless, to the authors' knowledge, there are only a few studies on this topic (Ghotbi & Taciroglu, 2020; Papadopoulos et al., 2020; Zhu et al., 2017). (Ghotbi & Taciroglu, 2020) proposed a new framework for aftershock probabilistic seismic hazard analysis (APSHA) and computed aftershock hazard curves for the given mainshock scenario. They used information from hazard disaggregation for a site in California to select hazard-consistent aftershock ground motion records using the generalized intensity measure (GCIM) approach (Bradley, 2010). (Zhu et al., 2017) developed a method for generating aftershock Conditional Mean Spectrum (CMS) using a copula technique, NGA-West2 (NGA West 2 | Pacific Earthquake Engineering Research Center (berkeley.edu)) ground motion database and (Abrahamson et al., 2014) ground motion prediction model (GMPM) to model the correlation between the MS and AS spectral ordinates. However, they only provide the correlation coefficients at the same period (T_{AS}=T_{MS}). In contrast, (Papadopoulos et al. 2020) empirically derived correlation coefficients by investigating the correlation of MS-AS spectral accelerations at different periods and proposed a pragmatic procedure that can be applied for the selection of MS-AS ground motion pairs using consistent causal parameters and accounting for the correlation between their spectral accelerations.

This report provides an upgrade of the Papadopoulos' methodology. We use a large database of ground motion recordings compiled in D5.1 to identify seismic sequences and investigate the proposed spectral acceleration correlation coefficient matrix. Finally, we present an example of how this MS-AS record selection methodology can be applied to a test site in Central Italy.

1. Definition of ground motion "site-specific rock-hazard-consistency" for clustered seismicity

As mentioned earlier, the proposed hazard-consistent record selection technique for clustered seismicity follows the work of (Papadopoulos et al. 2020) and it involves four main steps, as described below.

1. Mainshock record selection

The first step involves selecting MS records using the CS approach. One can adopt the methodology proposed by (Bradley, 2012) as explained in Section 1.2 of D5.1. With this approach, records are selected to match the target distribution in terms of spectral ordinates conditioned on the chosen intensity measure *IM** (e.g. *Sa*(T_1), *AvgSa*) for the hazard level of interest extracted from the corresponding hazard curve. Seismic hazard disaggregation is then performed to identify the scenarios (in terms of magnitude M, distance R and residual ε for the chosen *IM** level) that contribute to the exceedance of that *IM** level. For every scenario, we can then compute the mean and standard deviation of the natural logarithm of the spectral ordinates as:

$$\mu^i_{lnS_a|lnS_a(T^*)} = \mu^i_{lnS_a(T)} + \rho(T^*)\varepsilon_i\sigma^i_{\ln(S_a)} \quad (1)$$

$$\sigma^i_{\ln(S_a)|lnS_a(T^*)} = \sigma^i_{\ln(S_a)}\sqrt{1-\rho(T^*)^2} \quad (2)$$

where i represents the scenario, $\mu^i_{lnS_a(T)}$ and $\sigma^i_{\ln(S_a)}$ are the unconditional logarithmic mean spectral accelerations and associated standard deviations obtained from the GMPM, $\rho(T^*)$ represents the correlation coefficient between the residuals of the *IM** and *Sa*(T) across all periods of interest, which can be calculated with (Baker & Jayaram, 2008) or (Abrahamson et al., 2014) correlation structure. Every i^{th} scenario is associated with a weight, p_i, obtained from the disaggregation, which is then used to compute the target conditional mean and standard deviation of spectral accelerations *Sa*(T) given *IM**, by combining all scenarios as follows:

$$\mu_{lnS_a|\ln(IM^*)} = \sum_i \frac{p_i}{\bar{p}}\left[\mu^i_{lnS_a(T)|\ln(IM^*)}\right] \quad (3)$$

$$\sigma_{lnS_a|\ln(IM^*)} = \sqrt{\sum_i \frac{p_i}{\bar{p}}\left[\sigma^{2\,i}_{\ln(S_a)|\ln(IM^*)} + \left(\mu^i_{lnS_a(T)|\ln(IM^*)} - \mu_{lnS_a|\ln(IM^*)}\right)^2\right]} \quad (4)$$

where the quantity $\bar{p}$ is the sum of all the weights for the considered scenarios.

For every record that we want to select (for a total of, say, N_{rec}), we then randomly draw a rupture scenario (M and R) from the seismic disaggregation probability mass function for that *IM** level, and for the given i^{th} rupture we create the conditional spectrum with mean $\mu^i_{lnS_a(T)|\ln(IM^*)}$ and standard deviation $\sigma^i_{lnS_a|\ln(IM^*)}$. We then generate a random realization by sampling correlated *lnSa* values from the multivariate normal distribution and select a record (usually scaled) from an available database that best matches this realization. The process is repeated for every record *r*, ensuring that each one is associated with the previously drawn rupture scenario. This is crucial information for the next step of the framework, and it is the main reason why we do not use the procedure proposed by (Jayaram et al., 2011) described in Section 1.1 of D5.1. The simulation procedure is repeated several times and the set of records that best matches the target (given by Equations (3) and (4)) is selected. The accuracy of the matching to the target is calculated using the following SSE_s metric:

$$SSE_s = \sum_{k=1}^{p}\left[\left(m_{lnIM_k} - \mu_{lnIM_k}\right)^2 + w\left(s_{lnIM_k} - \sigma_{lnIM_k}\right)^2\right] \quad (5)$$

where m_{lnIM_k} is the sample mean of $lnIM_k$ and s_{lnIM_k} is the sample standard deviation of $lnIM_k$ values of the selected motions. The quantities μ_{lnIM_k} and σ_{lnIM_k} are the target conditional means and standard deviations, p is the number of oscillator periods of interest, and w is a weight factor that assigns relative importance to the mismatches in the mean versus standard deviation values. Once the initial set of records is selected, one can perform the so-called "greedy" optimization (Jayaram et al., 2011) to improve the match to the target by following the steps below:

a) Calculate the SSE_s metric for the initial set of selected records;

b) Set j=1

c) Sample N new rupture scenarios from the disaggregation probability mass function, generate N corresponding realizations of response spectra and match a new record r_{new} to every realization;

d) For every r_{new}, replace record r_j in the initial set with it and re-calculate the SSE_s metric. If the match has improved (i.e., the SSE_s is lower) keep the new record and replace the stored M and R associated with the record r_j with the M and R associated with r_{new}.

e) Set j=j+1 and repeat the previous steps as long as j≤N_{rec}.

This method, however, has a caveat. The M and R values of any mainshock response spectrum are indeed consistent with the M-R probability mass function extracted from the seismic hazard disaggregation but the M and R of the record selected to match it are not. Therefore, this procedure leads to records that have hazard-consistent spectral contents but are not necessarily consistent with the hazard in terms of other ground motions characteristics, such as duration, that may also affect the structural response.

To solve this issue, an alternative CS-MR method proposed by Spillatura et al. (2021) could be used for record selection. The CS-MR method selects the ground motions that not only match the target CS but are also faithful to the M-R distribution derived from hazard disaggregation. The selection process ensures that the percentage of ground motions from a given M-R bin chosen to match the target CS corresponds to the contribution of that bin to the hazard. For example, if 40 ground motions are sought to match a $Sa(T)$ – based CS and the contribution to the occurrence of that $Sa(T)$ level is 20% from M-R bin 1, 50% from bin 2 and the remaining 30% from bin 3, then the algorithm will pick 8, 20 and 12 records from bins 1, 2 and 3, respectively. In this manner, CS-MR effectively discards ground motions from earthquake scenarios that are unlikely to occur at the site, resulting in a set of response spectra that not only match the target distribution of spectral ordinates but also represent the ground motions that may actually occur at the site. Furthermore, IMs other than spectral ordinates are accounted for implicitly by the CS-MR method. The limitation of the method is the often limited number of records available in certain M-R bins. Additionally, one should keep in mind that selected ground motions are usually scaled which means that there might be a discrepancy between the scaled spectrum and the spectrum of the ground motions that are naturally produced by earthquakes with the given causative parameters.

2. Generation of aftershock sequences

The second step involves generating realistic aftershock sequences using the M and R values of each selected MS ground motion. There are different ways to accomplish this. Following (Papadopoulos et al. 2020) one can use the Epidemic-Type Aftershock Sequence (ETAS) model (Ogata, 1988) to generate sequences assuming that the MS is the parent event. Then one can sample the number of direct offspring from the productivity function (Poisson distribution with the mean number of offspring events k given in Equation (6) for the mainshock with magnitude m_i), their location from the spatial distribution estimating the distance r from the mainshock with magnitude m_i, and the angle θ (the polar coordinate) with Equation (7) and inter-arrival time Δt between parent and offspring event from Equation (8). The magnitude of each sampled aftershock event is sampled using the Gutenberg-Richter (GR) law and Equation (9).

The quantities A, a, p, c, D, q, γ and b are ETAS parameters whose values can be estimated using the maximum likelihood estimation method (MLE), u_r, u_θ, u_m and u_t are uniformly distributed random variables over the range (0, 1), while m_{min} is the minimum magnitude considered. Once we have the first generation of triggered events, we assume that these events can trigger offspring of their own using the same set of Equations (6) – (9). The simulation is repeated until the process dies out, i.e. until there are no new events triggered or the triggered events are outside the spatiotemporal window of our interest (say, one month or one year).

$$k(m_i) = Ae^{a(m_i - M_{min})} \tag{6}$$

$$r(m_i) = d\,e^{(m_i - M_{min})}\sqrt{u_r^{\frac{1}{1-q}} - 1},\ \theta = 2\pi u_\theta \tag{7}$$

$$\Delta t = -c + c(1-u_t)^{1/(1-p)} \quad (8)$$

$$m_{AS} = -\ln\frac{(1-u_m)}{bln10} + m_{min} \quad (9)$$

A simpler option would be to use the generalized Omori model (Shcherbakov et al., 2005) to simulate the sequences based on the number of events, their magnitude, and time stamp for the given mainshock record and associated causal parameters. To perform the simulation, the number of triggered events is drawn from the Poisson distribution with the mean number of events given in Equation (10).

$$k(m_i) = 10^{a+b(m_i-m_{min})}c^{(1-p)/(p-1)} \quad (10)$$

The timestamp and magnitude of the triggered events are computed using Equations (8) and (10), respectively. As in most cases mainshocks are identified as the events with the largest magnitude in the cluster, for consistency, the maximum aftershock magnitude is set not to exceed the magnitude of the triggering mainshock.

In the case of the Omori model, the parameters that have to be estimated are *a*, *c*, *p*, and *b*. It is worth noting that the literature provides different values of the ETAS and Omori parameters, which depend on the region of interest and the quality of the available data used for calibration (Seif et al., 2017; Šipčić et al., 2022). It is crucial to highlight that the values of the set of Omori parameters differ from those estimated in the ETAS model because the values of the Omori parameters embedded in ETAS are applied locally to every generation of aftershocks. On the other hand, in the generalized Omori law model, all aftershocks are assumed to be triggered by a single MS event and, therefore, the parameter values refer to entire sequences.

To simplify the process even further, one can assume that the entire sequence of events can be represented by a single aftershock with, on average, a magnitude m_{AS}=m_{MS}-1.2 (Båth, 1965). Since the generalized Omori law and Bath's law models do not consider the spatial distribution of aftershocks, one can assume that aftershocks occur within a circular area around the mainshock with a radius equal to three rupture lengths estimated using the scaling law of (Wells & Coppersmith, 1994). Alternatively, one can assume that the epicenter locations of the mainshock and aftershock are the same, as done in previous studies (e.g., Goda & Taylor, 2012; Yeo & Cornell, 2009).

3. Derivation of the mainshock consistent target aftershock spectrum (MSAS-CS)

For the given MS and AS ruptures (obtained in the first two steps), to select the AS GMs it is first necessary to find the distribution of the AS spectral accelerations at different periods of vibration that are conditional on the spectral accelerations of the specific MS record. To do so we use the MSAS-CS technique developed by (Papadopoulos et al., 2020). As shown by (Baker & Jayaram, 2008) for individual records and confirmed later by (Papadopoulos et al., 2019) for MS-AS pairs, the joint distributions of spectral accelerations at multiple periods is well represented by a multivariate lognormal distribution. The unconditional mean and variance-covariance matrix of the joint MS-AS log-spectral acceleration distribution are found using Equations (11) and (12). The conditional (on the MS spectral ordinates) mean and variance-covariance matrix for the AS ground motion are given by Equations (13) and (14).

$$\mu_0 = \mu_{01}|\mu_{02} = \left[\mu_{lnS_a(T_1^{AS})},\mu_{lnS_a(T_2^{AS})},\dots\mu_{lnS_a(T_n^{AS})}\right] | \left[\mu_{lnS_a(T_1^{MS})},\mu_{lnS_a(T_2^{MS})},\dots\mu_{lnS_a(T_n^{MS})}\right] \quad (11)$$

$$\Sigma_o = \left[\frac{\Sigma_{11}|\Sigma_{12}}{\Sigma_{21}|\Sigma_{22}}\right] \quad (12)$$

$$\mu_c' = \mu_{01}' + \Sigma_{12}\Sigma_{22}'(\mathrm{x}^{\mathrm{MS}} - \mu_{02}') \quad (13)$$

$$\Sigma_c = \Sigma_{11} + \Sigma_{12}\Sigma_{22}'\Sigma_{21} \quad (14)$$

where x^{MS} is the vector of observed MS logarithmic spectral accelerations, $\mu_{lnS_a(T_i)}$ and $\sigma_{lnS_a(T_i)}$ are unconditional mean and standard deviation of the spectral accelerations extracted from the GMPM. To find the covariance matrix it is necessary to have $\rho(T_i, T_j)$, which represents the correlation

coefficient between the logarithmic spectral accelerations at T_i and T_j of either MS or AS GM. More specifically, to find Σ_{11} and Σ_{22} it is necessary to have $\rho(T_i^{AS}, T_j^{AS})$ and $\rho(T_i^{MS}, T_j^{MS})$, respectively, and such quantities can be found using the model proposed by (Baker & Jayaram, 2008) or (Abrahamson et al., 2014), similarly as done in the first step of the process. To evaluate Σ_{12} and Σ_{21} we need $\rho(T_i^{AS}, T_j^{MS}), \rho(T_i^{MS}, T_j^{AS})$, which that can be found using the correlation structure described in Section 3 of this Report. For more details regarding the MSAS-CS procedure briefly discussed here, see (Papadopoulos et al. 2020).

4. Selection of the aftershock GMs

Having the MS-consistent AS target, a realization of the AS response spectrum is sampled from the joint AS *Sa* distribution followed by the selection of the ground motion (which is usually scaled) that best matches the target spectrum (i.e., it has the lowest sum of the squared errors across periods). For computational simplicity, only one realization of the AS ground motion is drawn. As many selected AS ground motions will have very low intensity, one can set a threshold below which all sampled GMs are discarded and the simulation is repeated. As shown by (Papadopoulos et al. 2020) the potential bias is not expected to be of importance as long as the intensity threshold for discarding is kept reasonably low, i.e., the small magnitude and/or large distance MS ruptures are not forced to produce AS sequences with unrealistically large M and associated ground motions.

In the following sections, we first use the database of GMs assembled in Task 5.1.4 of WP5 to identify the seismic sequences (MS-AS recording pairs). Subsequently, we compare the spectra of the real recorded sequences from our assembled database with those determined by the (Papadopoulos et al., 2019) correlation structure. Section 3 of this report provides an example of the record selection framework described above using CS for MS record selection and the Omori model for generating seismic sequences for the given mainshock causative parameters.

2. Assembling the database of ground motion sequences

To form the mainshock-aftershock ground motion pairs we make use of a database that was compiled as described in D5.1. Figure 2 shows the epicenters of the earthquakes that caused the ground motions included in the database while Figure 3 depicts the structure of the mat file that contains all ground motions (34107 3-component records).

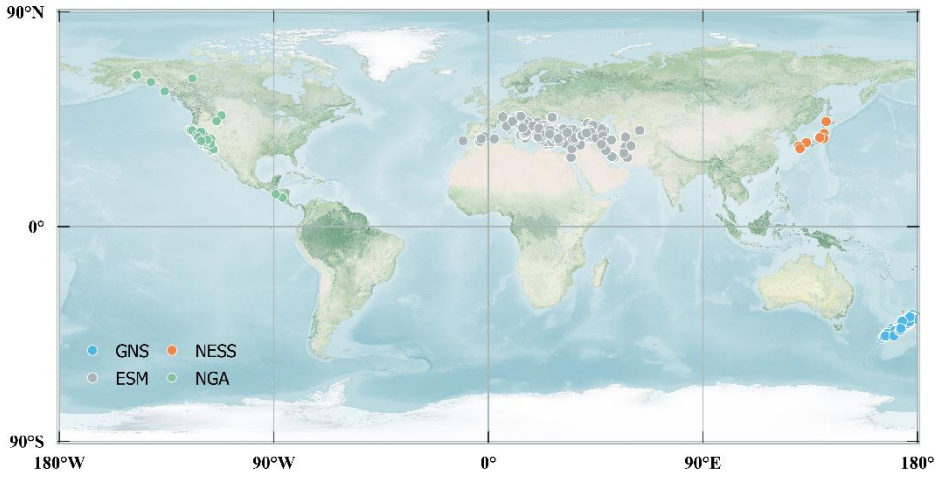

Figure 2: Map of epicenters of the earthquakes that caused the ground motions included in the assembled dataset, color-coded based on the original databases.

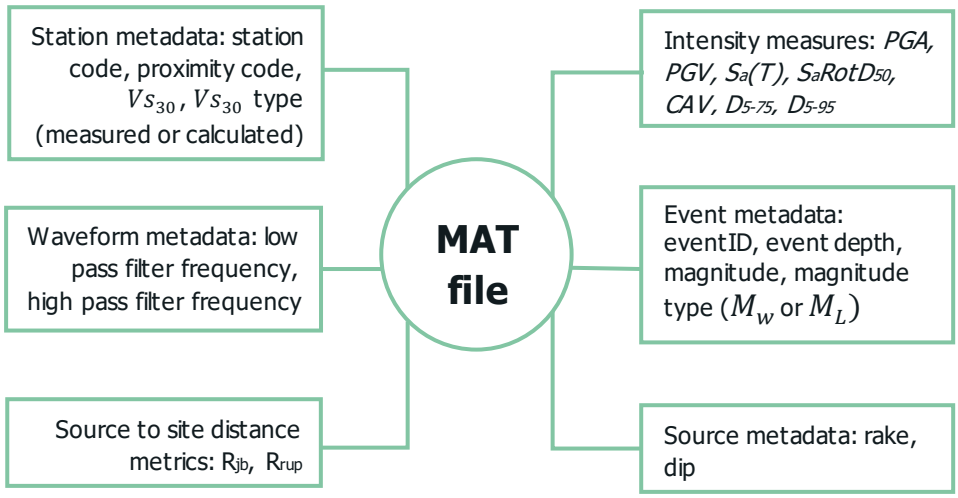

Figure 3: Schematic structure of the MAT file that contains all considered ground motions.

As a part of our analysis, we explored three declustering methods available in the literature, namely (Gardner & Knopoff, 1974), (Reasenberg, 1985), and (Zaliapin et al., 2008). The most used and simplest technique for identifying seismic sequences is the window-based (Gardner & Knopoff, 1974) method. The algorithm identifies the largest magnitude event in a sequence and removes all other events within a window with M-specific pre-specified temporal and spatial parameters centered at the identified event. A more complex declustering approach was later proposed by (Reasenberg, 1985) who expanded on the work of (Savage, 1972). Their idea was to link every event to a cluster via a spatiotemporal proxy. Every event linked with the prior one joins its cluster and subsequently, clusters grow by association. Thus, the spatiotemporal window does not solely depend on the mainshock magnitude but instead varies with events' behavior. More precisely, the spatial extension is based on the stress distribution pattern, which is assumed to depend on the cluster's last and largest event. The temporal extension is developed based on the probabilistic model and Omori law. More details about the model can be found in (Molchan & Dmitrieva, 1992; Reasenberg, 1985; Stiphout et al., 2012). Finally, we use the nearest-neighbor proxy defined by (Zaliapin et al., 2008) to identify the sequences, the largest magnitude event of which is kept as the mainshock. We developed Python scripts that can be used to classify events as either foreshock, mainshock, or aftershock with these three different methods.

One should bear in mind that the results of these declustering methods are affected by the values of the parameters utilized to define them, whose values are calibrated based on a particular region and, often, based on a limited amount of data. These values may or may not be the optimal set of parameters' values for regions different from those were they were created but are nonetheless used extensively and somewhat ubiquitously in the literature. Besides the three considered here, several other methods for identifying sequences can be found in the literature, from simple deterministic ones to more advanced stochastic ones such as (Llenos & Michael, 2020; Zaliapin & Ben-Zion, 2020; Zhuang et al., 2004). This high number of available declustering methods clearly reflects the true difficulties and somewhat the arbitrariness implicit in the classification of earthquake events.

After categorizing the events as either MS or AS, we extracted the MS-AS ground motions pairs that are identified as those belonging to the same sequence and are recorded at the same station. Figure 4 shows the peak ground acceleration (PGA) of the identified MS-AS pairs, obtained with the (Gardner & Knopoff, 1974) algorithm. In only 7% of the cases the PGA of the AS is higher than that of the MS. Events illustrated are from different databases, namely: the Engineering Strong-Motion (ESM) database (https://esm-db.eu) (Lanzano et al., 2019), NGA-West2, Ridgecrest sequence (Rekoske et al., 2019) and New Zealand Strong-Motion database (here referred to as GNS) (Van Houtte et al., 2017).

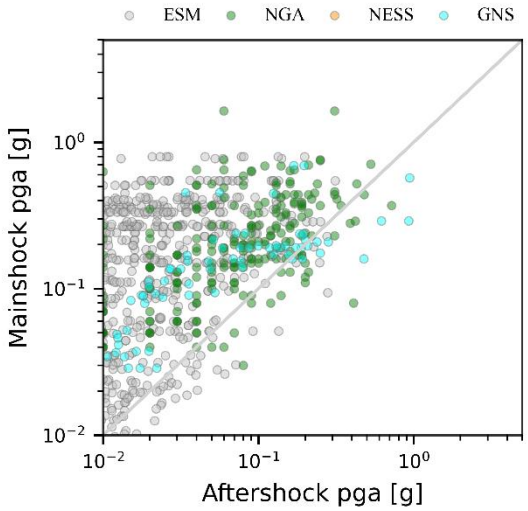

Figure 4 – PGA of the identified MS-AS recording pairs identified using the (Gardner & Knopoff, 1974) algorithm

3. Statistical correlation between the IMs of mainshock – aftershock ground motion pairs

(Papadopoulos et al., 2019) developed the correlation model between the spectral accelerations of MS and AS ground motions by utilizing the NGA-WEST2 database and the GMPM of (Abrahamson et al., 2014) (ASK14) to extract the residuals. After identifying sequences, as explained in (Wooddell & Abrahamson, 2014), they assembled 1146 MS-AS recording pairs from 48 sequences. Their study investigated the inter-period spectral acceleration correlation coefficients of AS ground motions and compared them to estimates derived from MS recordings, finding some mild differences that could not be attributed to the intrinsic differences between AS and MS ground motions. That study also estimated empirical correlation coefficients between MS and AS spectral accelerations, including the cross-correlation between MS spectral accelerations at T_{MS} and AS spectral accelerations over the entire period range of interest, and provided parametric predictive equations for their computation. The results showed that AS spectral accelerations are mildly correlated with their mainshock counterparts for closely-spaced periods of vibration and weakly correlated over the rest of the period range. They showed that assuming the bivariate normality of MS and AS residuals is a reasonable choice.

Figure 5 compares the unconditional and conditional mean aftershock spectra with the spectra of the recorded aftershock ground motion for two cases, one extracted from the ESM database and the other from the GNS database. The effect of the positive correlation between the spectral acceleration of the MS and the AS recordings is clear. Figure 6 shows instead the error term, defined as the ratio of the difference between predicted and observed lnSa over the observed value of lnSa. It is apparent that the discrepancy between the spectrum of the real aftershock motion and that of the ground motion predicted using the proposed methodology is significantly reduced compared to the discrepancy of the aftershock motion predicted based only on the M and R of the aftershock (i.e., calculated using the GMPM only). Even though the error is reduced it is still higher than one might have expected. This is likely related to the fact that (Papadopoulos et al., 2019) calibrated the correlation coefficients based on the NGA-West2 database where some characteristics of the ground motions (e.g., V_{s30}, depth at which the profile reaches a velocity of 1.0 km/s ($Z_{1.0}$), etc.) are often either completely missing or have values that differ significantly from the ones in ESM and GNS database.

(a) (b)

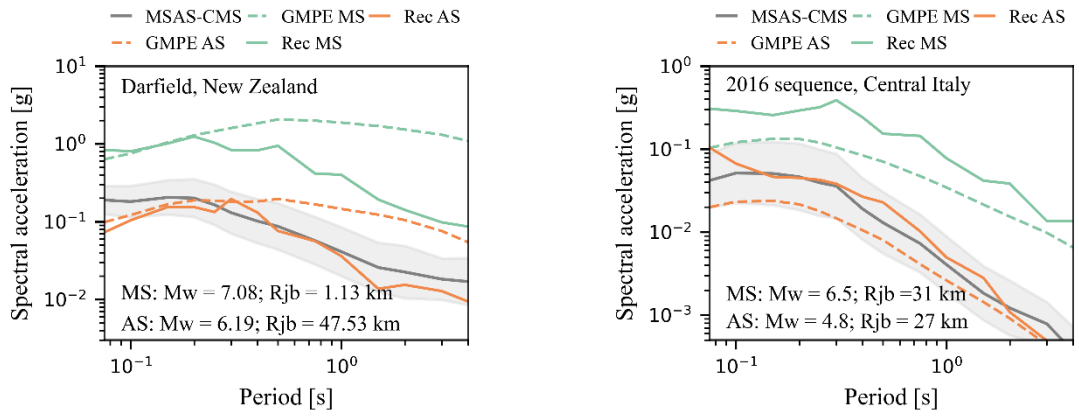

Figure 5 – Comparison between recorded (MS and AS), unconditional (obtained with only the GMPM), and conditional AS spectra (MSAS-CMS) of ground motions for MS-AS pairs from (a) Darfield sequence and GNS database and (b) Central Italy 2016 sequence and ESM database. The shaded area corresponds to ±2 standard deviations.

(a) (b)

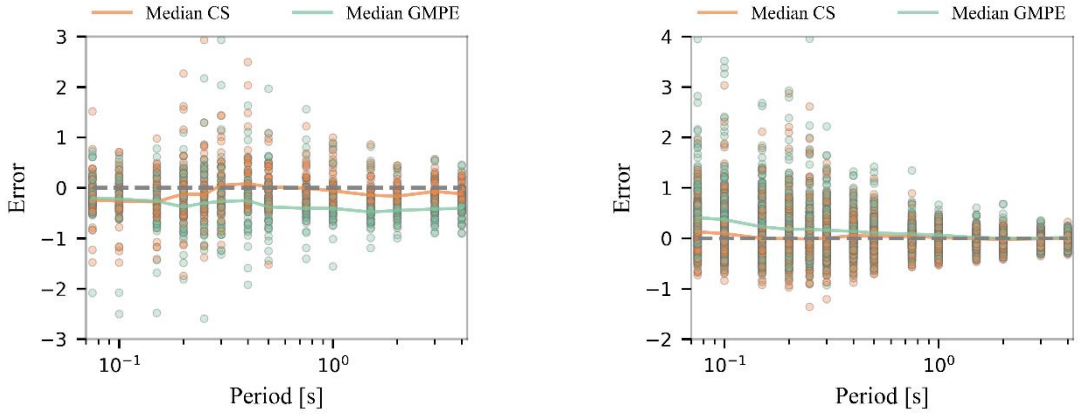

Figure 6 – Distribution of the error calculated as the ratio of the difference between the predicted and observed (recorded) ln*Sa* over the observed value of ln*Sa*. For comparison, predicted values are calculated with the proposed MS-consistent CS and with the ASK14 GMPM only. (a) GNS and (b) ESM database. Legend: median CS=median error based on the conditional approach used here; median GMPM= median error based on the GMPM prediction.

4. Ground motion hazard consistency for clustered seismicity – example

To illustrate the MS-AS record selection procedure, we selected a site in Perugia, Central Italy (Figure 7), located at 43.11°N and 12.39°E on the rock with V_{s30}=800 m/s. We defined 10 intensity measure levels (*IMLs*) of increasing intensity that correspond to values ranging between 0.2% probability of

exceedance (poe) in 50 years (i.e., return period of 25000 years) to 70% poe in 50 years (i.e., return period of 40 years) using *Sa*(0.26s) as conditioning *IM*. We performed PSHA for the selected site to identify the *IMLs* corresponding to the desired poe's (Table 1). For the calculations, we used the (Boore & Atkinson, 2008) GMPM, the area source model developed for the SHARE[2] project, and the OpenQuake software (Pagani et al., 2014). We then performed the seismic hazard disaggregation analysis to identify the events (in terms of their magnitude and distance) contributing to the hazard at each intensity level.

Figure 7 - Location of the site used as a case study

IML	poe in 50 years [%]	$Sa(0.26s)$
1	70	0.16
2	50	0.22
3	30	0.29
4	10	0.50
5	5	0.68
6	2	0.98
7	1.5	1.10
8	1	1.27
9	0.6	1.52
10	0.2	2.13

Table 1: Values of the *Sa*(0.26s) at the 10 poe levels at the Perugia site.

For each *IML* we selected 22 MS GMs to match the target CS spectrum, following the methodology described in Section 1. Each MS record is associated with rupture parameters M and R. Note that CS-MR was not used here because some M-R bins did not contain enough records to match the target spectrum well.

For each record associated with a MS earthquake, a sequence of AS events is simulated using the Omori model, Equations (8) – (10), and parameters calibrated for the region in Central Italy (Šipčić et al., 2022). The location of the aftershocks is modeled using the (Wells & Coppersmith, 1994) scaling law. For every AS in the sequence, we defined the target spectrum of the ground motion at the Perugia site using the Papadopoulos et al. methodology. We consider only AS events that are triggered in the period of one year after the MS and within a radius of 100 km. Only ground motions with *Sa*(0.26s) higher than 0.2g are retained. As an example, let us consider the *IML*4 and the 22 MS records selected for that hazard level. Table 2 shows the magnitude (M_w) and distance (R_{jb}) of each MS event, the number of simulated AS events, the maximum AS magnitude and the corresponding distance from the epicenter to the site.

MS ID	MS M_w	MS R_{jb}	# of AS	Max AS M	AS R_{jb}

[2] www.share-eu.org

1	7.25	25	7	7.1	35
2	5.25	5	4	5.1	2
3	6.25	5	7	6.1	5
4	6.25	5	2	5.5	3
5	7.25	5	2	6.5	16
6	7.25	45	1	5.6	42
7	6.25	55	1	5.5	54
8	7.25	15	1	5.0	3
9	6.75	5	4	6.2	3
10	6.75	15	1	5.3	8
11	6.75	25	8	6.0	23
12	6.25	5	7	6.2	25
13	6.25	5	1	4.3	5
14	6.75	15	2	5.8	5
15	6.75	35	31	6.6	33
16	6.25	5	5	6.0	15
17	6.25	35	8	6.2	32
18	5.75	5	2	5.4	3
19	7.25	5	1	5.2	5
20	7.25	15	15	6.7	18
21	6.25	15	2	5.5	5
22	7.25	5	5	6.2	2

Table 2: MS records selected for *IML4*, their magnitude M, distance R, number of simulated aftershock events, maximum magnitude of the simulated aftershock events and corresponding distance to the site.

Figure 8a shows the response spectrum of the first selected MS record for *IML4* with M_w 7.25 and R_{jb} of 25km, which triggered seven AS events. The spectrum of the AS with the largest magnitude (M_w 7.1 and corresponding distance R_{jb} 35km) is illustrated in the same figure. As one can see, the spectrum of the MS ground motion is above the median spectrum predicted by the GMPM for that M and R and, therefore, the target AS spectrum is also above the median AS GMPM spectrum due to the MS-AS *Sa* positive correlation.

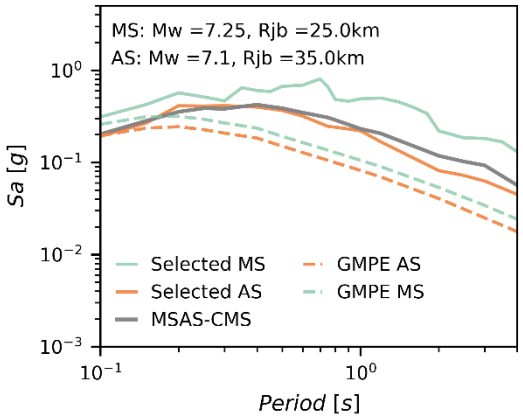

Figure 8 – Response spectra of the selected MS and AS ground motions, the median prediction of the MS and AS ground motion spectra based on GMPM only and the median prediction of the aftershock ground motion spectrum MSAS-CS conditional on the MS rupture and MS ground motion. The figure displays the first selected MS record from Table 2 and the AS GM corresponding to the largest triggered AS (i.e., M7.1 at 35km).

5. Conclusions

To support ground motion record selection in the METIS project, in the context of clustered seismicity, we recommend implementing the mainshock-consistent aftershock record selection scheme proposed by (Papadopoulos et al., 2020). We described the recommended framework that includes the following three steps:

1. the selection of mainshock ground motions (using the Conditional Spectrum approach),
2. the generation of realistic aftershock events for the given mainshock rupture, using the ETAS or Omori model. One should keep in mind the former is more sophisticated, but the latter is consistent with the hazard model developed within WP4; and
3. the derivation of the mainshock-consistent aftershock target ground motion spectrum (using the correlation coefficients between the mainshock and aftershock ground motion spectral ordinates and the causative parameters of the associated mainshock and aftershock events).

The selection of mainshock ground motions is performed individually and different approaches can be used as long as the M and R information are stored for each selected ground motion, as they are used to generate AS events in Step 2 above. That said, we described two methods that can be used for MS ground motion selection: the one proposed by (Papadopoulos et al., 2020) and the CS-MR method proposed by Spillatura et al. (2021). To generate realistic AS events for the given MS event models such as ETAS, modified Omori or simple Bath's law can be utilized.

As an illustrative example, we applied the described methodology to a case study in Perugia, Central Italy, for which the seismic hazard was computed via OpenQuake. We considered ten levels of ground motion intensity covering values corresponding to a range of 0.2% to 70% poe in 50 years at the site. In the illustrated example we used $Sa(T_1)$ as the conditioning *IM*, however, other *IMs* could also be used (e.g., *AvgSa*) without significant changes in the methodology. In this example to select MS ground motions we applied the (Papadopoulos et al., 2020) methodology, while the AS events were generated using the Omori model with parameters' values calibrated for the Central Italy region.

It is important to note that while the proposed methodology ensures consistency between the MS and AS ground motions, there is no target distribution when it comes to selecting AS ground motions, i.e., we are sampling random AS ruptures and selecting corresponding AS ground motions. Therefore, to obtain robust response estimates for deriving damage state dependent fragility curves, it might be necessary to carry out a large number of analyses. However, we believe that using the proposed framework is a reasonable compromise because deriving a target AS ground motion distribution would require performing either vector (MS-AS) PSHA or aftershock PSHA for every selected MS record, which

are time-consuming tasks that we feel are unnecessarily complicated for the purpose of this NPP-centered study.

When the hazard results will become available for the NPP site in central Italy (see WP3), this procedure will be repeated for that site. The selected mainshock-aftershock suites of records that will be obtained for that site can then be used in WP6 to estimate the damage-dependent fragility curves of systems, structures and components of nuclear power plants for the METIS case study.

6. Acknowledgements

We want to thank Dr. Athanasios Papadopoulos for sharing the scripts for the mainshock-consistent aftershock ground motion record selection. Furthermore, we want to acknowledge suggestions and comments from him and from Professor Dimitrios Vamvatsikos that improved the quality of this study.

7. Bibliography

Abrahamson, N. A., Silva, W. J., & Kamai, R. (2014). Summary of the ASK14 ground motion relation for active crustal regions. *Earthquake Spectra*, *30*(3), 1025–1055. https://doi.org/10.1193/070913EQS198M

Aljawhari, K., Gentile, R., Freddi, F., & Galasso, C. (2020). Effects of Ground-motion Sequences on Fragility and Vulnerability of Case-Study Reinforced Concrete Frames. In *Bulletin of Earthquake Engineering: Vol. under rev* (Issue 0123456789). Springer Netherlands. https://doi.org/10.1007/s10518-020-01006-8

Amadio, C., Fragiacomo, M., & Rajgelj, S. (2003). The effects of repeated earthquake ground motions on the non-linear response of SDOF systems. *Earthquake Engineering and Structural Dynamics*, *32*, 291–308. https://doi.org/10.1002/eqe.225

Baker, J. W., & Jayaram, N. (2008). Correlation of spectral acceleration values from NGA ground motion models. *Earthquake Spectra*, *24*(1), 299–317. https://doi.org/10.1193/1.2857544

Båth, M. (1965). Lateral inhomogeneities of the upper mantle. *Tectonophysics*, *2*(6), 483–514.

Boore, D. M., & Atkinson, G. M. (2008). Ground-motion prediction equations for the average horizontal component of PGA, PGV, and 5%-damped PSA at spectral periods between 0.01 s and 10.0 s. *Earthquake Spectra*, *24*(1), 99–138. https://doi.org/10.1193/1.2830434

Bradley, B. A. (2010). A generalized conditional intensity measure approach and holistic ground-motion selection. *Earthquake Engineering & Structural Dynamics*, *39*, 1321–1342. https://doi.org/10.1002/eqe

Bradley, B. A. (2012). A ground motion selection algorithm based on the generalized conditional intensity measure approach. *Soil Dynamics and Earthquake Engineering*, *40*, 48–61. https://doi.org/10.1016/j.soildyn.2012.04.007

Cornell, C. A., & Krawinkler, H. (2000). *Progress and challenges in seismic performance assessment* (pp. 1–3). PEER Center News, 3. https://apps.peer.berkeley.edu/news/2000spring/performance.html

Gardner, J. K., & Knopoff, L. (1974). Is the sequence of earthquakes in southern California with aftershocks removed, Poissonian? *Bulletin - Seismological Society of America*, *64*(5), 1363–1367.

Ghotbi, A. R., & Taciroglu, E. (2020). Conditioning criteria based on multiple intensity measures for selecting hazard-consistent aftershock ground motion records. *Soil Dynamics and Earthquake Engineering*, *139*, 106345. https://doi.org/10.1016/j.soildyn.2020.106345

Goda, K., & Taylor, C. A. (2012). Effects of aftershocks on peak ductility demand due to strong ground motion records from shallow crustal earthquakes. *Earthquake Engineering & Structural Dynamics*, *41*, 2311–2330. https://doi.org/10.1002/eqe

Jayaram, N., Lin, T., & Baker, J. W. (2011). A Computationally efficient ground-motion selection algorithm for matching a target response spectrum mean and variance. *Earthquake Spectra*, *27*(3), 797–815. https://doi.org/10.1193/1.3608002

Jeon, J.-S., DesRoches, R., Lowes, L. N., & Brilakis, I. (2015). Framework of aftershock fragility assessment-case studies: older California reinforced concrete building frames. *Earthquake Engineering & Structural Dynamics*, *44*(15), 2617–2636. https://doi.org/10.1002/eqe.2599

Kohrangi, M., Bazzurro, P., Vamvatsikos, D., & Spillatura, A. (2017). Conditional spectrum-based ground motion record selection using average spectral acceleration. *EARTHQUAKE ENGINEERING & STRUCTURAL DYNAMICS Earthquake*. https://doi.org/10.1002/eqe.2876

Lanzano, G., Sgobba, S., Luzi, L., Puglia, R., Pacor, F., Felicetta, C., D'Amico, M., Cotton, F., & Bindi, D. (2019). The pan-European Engineering Strong Motion (ESM) flatfile: compilation criteria and data statistics. *Bulletin of Earthquake Engineering*, *17*(2), 561–582. https://doi.org/10.1007/s10518-018-0480-z

Li, Q., & Ellingwood, B. R. (2007). *Performance evaluation and damage assessment of steel frame buildings under main shock – aftershock earthquake sequences*. *January*, 405–427. https://doi.org/10.1002/eqe

Li, Y., Song, R., & Van De Lindt, J. W. (2014). Collapse fragility of steel structures subjected to earthquake mainshock-aftershock sequences. *Journal of Structural Engineering*, *140*(12), 4014095. https://doi.org/10.1061/(ASCE)ST.1943-541X.0001019

Lin, T., Harmsen, S. C., Baker, J. W., & Luco, N. (2013). Conditional spectrum computation incorporating multiple causal earthquakes and ground-motion prediction models. *Bulletin of the Seismological Society of America*, *103*(2 A), 1103–1116. https://doi.org/10.1785/0120110293

Lin, T., Haselton, C. B., & Baker, J. W. (2013). Conditional spectrum-based ground motion selection. Part I: Hazard consistency for risk-based assessments. *Earthquake Engineering & Structural Dynamics*, *42*, 1847–1865. https://doi.org/10.1002/eqe

Llenos, A. L., & Michael, A. J. (2020). Regionally optimized background earthquake rates from ETAS (Robere) for probabilistic seismic hazard assessment. *Bulletin of the Seismological Society of America*, *110*(3), 1172–1190. https://doi.org/10.1785/0120190279

McGuire. (2004). *Seismic hazard and risk analysis*. Earthquake Engineering Research Institute, Oakland, U.S.A.

Molchan, G. M., & Dmitrieva, O. E. (1992). Aftershock identification: methods and new approaches. *Geophysical Journal International*, *109*(3), 501–516. https://doi.org/10.1111/j.1365-246X.1992.tb00113.x

Ogata, Y. (1988). Statistical Models for Earthquake Occurrences and Residual Analysis for Point Processes. *American Statistical Association*, *83*(401), 9–27.

Pagani, M., Monelli, D., Weatherill, G., Danciu, L., Crowley, H., Henshaw, P., Butler, L., Nastasi, M., Panzeri, L., Simionato, M., & Vigano, D. (2014). OpenQuake Engine : An Open Hazard (and Risk) Software for the Global Earthquake Model. *Seismological Research Letters*, *85*(3), 692–702. https://doi.org/10.1785/0220130087

Papadopoulos, A. N., Kohrangi, M., & Bazzurro, P. (2019). Correlation of spectral acceleration values of mainshock-aftershock ground motion pairs. *Earthquake Spectra*, *55*(1), 39–60. https://doi.org/10.1193/020518EQS033M

Papadopoulos, A. N., Kohrangi, M., & Bazzurro, P. (2020). *Mainshock-consistent ground motion record selection for aftershock sequences*. *January*, 754–771. https://doi.org/10.1002/eqe.3263

Raghunandan, M., Liel, A. B., & Luco, N. (2015). Aftershock collapse vulnerability assessment of reinforced concrete frame structures. *Earthquake Engineering & Structural Dynamics*, *44*(3), 419–439. https://doi.org/10.1002/eqe.2478

Reasenberg, P. (1985). Second-Order Moment of Central California Seismicity, 1969-1982. *JOURNAL OF GEOPHYSICAL RESEARCH*, *90*, 5479–5495.

Reasenberg, P. A., & Jones, L. M. (1989). Earthquake Hazard After a Mainshock in California. *Science*, *243*(4895), 1173–1176.

Rekoske, J., Thompson, E. M., Moschetti, M. P., Hearne, M., Aagaard, B. T., & (2019)., G. A. P. (2019).

Ground motions from the 2019 Ridgecrest, California, Earthquake Sequence. Center for Engineering Strong Motion Data (CESMD). https://doi.org/10.5066/P9REBW60.

Ruiz-García, J., & Negrete-Manriquez, J. C. (2011). Evaluation of drift demands in existing steel frames under as-recorded far-field and near-fault mainshock-aftershock seismic sequences. *Engineering Structures*, *33*(2), 621–634. https://doi.org/10.1016/j.engstruct.2010.11.021

Ryu, H., Luco, N., Uma, S. R., & Liel, A. B. (2011). Developing fragilities for mainshock-damaged structures through incremental dynamic analysis. *Proceedings of the Ninth Pacific Conference on Earthquake Engineering*, *Auckland*, *New Zealand*, 14-16 April.

Savage, W. U. (1972). Microearthquake clustering near Fairview Peak, Nevada, and in the Nevada Seismic Zone. *Journal of Geophysical Research*, *77*(35), 7049–7056. https://doi.org/10.1029/JB077i035p07049

Seif, S., Mignan, A., Zechar, J. D., Werner, M. J., & Wiemer, S. (2017). Estimating ETAS: The effects of truncation, missing data, and model assumptions. *Journal of Geophysical Research: Solid Earth*, *122*(1), 449–469. https://doi.org/10.1002/2016JB012809

Shcherbakov, R., Turcotte, D. L., & Rundle, J. B. (2005). Aftershock statistics. *Pure and Applied Geophysics*, *162*(6–7), 1051–1076. https://doi.org/10.1007/s00024-004-2661-8

Šipčić, N., Kohrangi, M., Papadopoulos, A. N., Marzocchi, W., & Bazzurro, P. (2022). The Effect of Seismic Sequences in Probabilistic Seismic Hazard Analysis. *Bulletin of the Seismological Society of America*, *Xx*, 1–16. https://doi.org/10.1785/0120210208

Spillatura, A., Kohrangi, M., Bazzurro, P., & Vamvatsikos, D. (2021). Conditional spectrum record selection faithful to causative earthquake parameter distributions. *Earthquake Engineering and Structural Dynamics*, *50*(10), 2653–2671. https://doi.org/10.1002/eqe.3465

Stiphout, T. Van, Zhuang, J., Marsan, D., Service, S. S., & Zurich, E. T. H. (2012). *Theme V – Models and Techniques for Analyzing Seismicity Seismicity Declustering*. *February*, 1–25. https://doi.org/10.5078/corssa-52382934.

Sunasaka, Y., & Kiremidjian, A. S. (1993). *A method for structural safety evaluation under mainshock-aftershock earthquake sequences* (Issue Report No. 105).

Van Houtte, C., Bannister, S., Holden, C., Bourguignon, S., & Mcverry, G. (2017). The New Zealand strong motion database. *Bulletin of the New Zealand Society for Earthquake Engineering*, *50*(1), 1–20. https://doi.org/10.5459/bnzsee.50.1.1-20

Wells, D. L., & Coppersmith, K. J. (1994). New empirical relationships among magnitude, rupture length, rupture width, rupture area, and surface displacement. *Bulletin - Seismological Society of America*, *84*(4), 974–1002.

Wen, W., Zhai, C., Ji, D., Li, S., & Xie, L. (2017). Framework for the vulnerability assessment of structure under mainshock-aftershock sequences. *Soil Dynamics and Earthquake Engineering*, *101*(April), 41–52. https://doi.org/10.1016/j.soildyn.2017.07.002

Wooddell, K. E., & Abrahamson, N. A. (2014). Classification of main shocks and aftershocks in the NGA-West2 database. *Earthquake Spectra*, *30*(3), 1257–1267. https://doi.org/10.1193/071913EQS208M

Yeo, G. L., & Cornell, C. A. (2009). A probabilistic framework for quantification of aftershock ground-motion hazard in California : Methodology and parametric study. *Earthquake Engng Struct. Dyn.*, *38*, 45–60. https://doi.org/10.1002/eqe.840

Zaliapin, I., & Ben-Zion, Y. (2020). Earthquake Declustering Using the Nearest-Neighbor Approach in Space-Time-Magnitude Domain. *Journal of Geophysical Research: Solid Earth*, *125*(4), 0–2. https://doi.org/10.1029/2018jb017120

Zaliapin, I., Gabrielov, A., Keilis-Borok, V., & Wong, H. (2008). Clustering Analysis of Seismicity and Aftershock Identification. *Physical Review Letters*, *101*(01), 015801. https://doi.org/10.1103/PHYSREVLETT.101.018501

Zhu, R. G., Lu, D. G., Yu, X. H., & Wang, G. Y. (2017). Conditional mean spectrum of aftershocks.

Bulletin of the Seismological Society of America, *107*, 1940–1953. https://doi.org/10.1785/0120160254

Zhuang, J., Ogata, Y., & Vere-Jones, D. (2004). Analyzing earthquake clustering features by using stochastic reconstruction. *Journal of Geophysical Research: Solid Earth*, *109*(5), 1–17. https://doi.org/10.1029/2003JB002879